COMPUTER SCIENCE
TECHNICAL REPORT SERIES

UNIVERSITY OF MARYLAND
COLLEGE PARK, MARYLAND
20742

TR-795
DAAG-53-76C-0138

July 1979

BLOB DETECTION BY RELAXATION

Alan Danker
Azriel Rosenfeld
Computer Vision Laboratory
Computer Science Center
University of Maryland
College Park, MD 20742

Abstract

A blob is a compact region lighter (or darker) than its background surrounded by a smoothly curved edge. Blobs can be detected using cooperating relaxation processes to enhance their interior and edge probabilities. A discussion of the processes working independently and together is given. The use of a pyramidal relaxation structure, the use of the closedness of contours as an additional information source, and the extension of cooperating relaxation processes to a time sequence of images are also discussed.

The support of the Defense Advanced Research Projects Agency and the U.S. Army Night Vision Laboratory under Contract DAAG-53-76C-0138 (DARPA Order No. 3206) is gratefully acknowledged, and is the help of Kathryn Riley in preparing this paper. This paper is based on the first author's M.S. thesis (University of Maryland, 1979). Thanks are also due to Chuck Dyer for critical suggestions, Russ Smith for his relaxation software and for implementing the borderness scheme, and Sanjay Ranade for his efforts on the pyramid project.

PREFACE

Basic to most image understanding tasks is the segmentation of objects from their background. In simple situations the objects to be extracted may be "blobs". A blob can be characterized as a compact region lighter (or darker) than its background surrounded by a smoothly curved edge. In principle, a blob can be extracted by thresholding the image at an appropriate level, or its bounds can be defined by an edge detector. However, because of noise and blur, pure object/background discrimination can rarely be achieved in this way. This thesis poses a fuzzy classification scheme for blob detection. It incorporates ideas used in non-probabilistic methods making use of edge/border coincidence, and implements these ideas in the form of a probabilistic relaxation process.

In Chapter I probabilistic relaxation is discussed and blob detection using edge/border coincidence is described.

In Chapter II the behavior of the edge process and the gray level process are examined, first when operating separately and then when interacting in a joint relaxation process.

Chapter III discusses several extensions to the blob extraction processes. These include a pyramid structure for multilevel relaxation, the use of curvature information as a basis for the initial estimation of "inside" and "outside" class probabilities, and a scheme for computing compatibility coefficients for detecting objects in a time sequence of one-dimensional images.

CHAPTER I

BACKGROUND

1.1 Probabilistic Relaxation

A primary step in the analysis of an image is the discrimination or classification of the parts of the image. A low level symbolic description of the image based on local evidence (i.e., gray level, gradient magnitude, curvature) can be built. However, local evidence may be misleading, causing ambiguities in the classification. Ambiguities arise from the sensitivity of local evidence to noise, or multiple responses to the same gray level pattern, as in computing slope information. The ambiguity problem is especially severe if the classification is done in parallel with each point being classified without reference to any classification decisions that may have already been made at other points. To disambiguate the classification, an iterative process which makes use of the relationships among the classes to reduce or eliminate the ambiguity is employed. This computational process is called "relaxation labeling" [1].

The relaxation labeling method uses probabilistic classification rather than making firm classification decisions immediately. Classification probabilities at a given iteration are allowed to depend on decisions made at the previous iteration.

The probability updating at a given iteration is done in parallel over the entire image.

To convey the general idea of the method, a simplified overview is given in [2]. We initially assign to each point P the probability p_i that it belongs to each of its possible classes. We then examine the probabilities at neighboring points, increasing p_i if supporting evidence is found for it (i.e., if there exist high probabilities that the neighbors of P have compatible classifications), or decrease it if contradictory evidence is found (i.e., there exist high probabilities of incompatible classification at P's neighbors). The updating is done in parallel for every P and every p_i, and the process can be iterated as many times as desired.

Two formal models of the process have been formulated and applied [3][4]. We now briefly describe the models. Let $A = \{a_1,\ldots,a_n\}$ be the set of objects (possibly single points) in a scene, each of which belongs to one of the classes of the set $\Lambda = \{\lambda_1,\ldots,\lambda_m\}$. With each a_i we associate a probability vector $(p_{i1},\ldots,p_{im})$, where p_{ik} is an estimate of the probability that a_i belongs to the class λ_k, where $\sum_{\lambda=\Lambda} p_i(\lambda) = 1$, and $0 \leq p_i(\lambda) \leq 1$ for all $a_i \in A$. This estimate is based on some conventional analysis of a_i. For example, the initial estimate of the edgeness of the point a_i may be proportional to the magnitude of the gradient of the image at a_i. For each pair of neighboring objects a_i, a_j (given a specified neighbor

relation) and each pair of classes λ_h, λ_k, there is a measure of compatibility between object a_i belonging to class λ_h and object a_j belonging to class λ_k. Compatibilities are given by the function $r_{ij}(\lambda,\lambda')$ where $-1 \leq r \leq +1$ and

a) if λ at a_i is compatible with λ' at a_j, then $r_{ij}(\lambda,\lambda') > 0$;

b) if λ at a_i is incompatible with λ' at a_j, then $r_{ij}(\lambda,\lambda') < 0$;

c) if neither labeling is constrained by the other ("don't care" situation), then $r_{ij}(\lambda,\lambda') = 0$;

d) the magnitude of r_{ij} represents the strength of the compatibility.

Compatibility coefficients can be computed as correlation functions, by a priori evaluation of the ways in which the classes can interact, or based on mutual information of the labels at neighboring points (i.e., if two labels have a high positive correlation, it is expected that they will have a high mutual information, and vice versa). The pairwise compatibilities among the labels at adjacent points computed by mutual information are estimated using ratios of probabilities given by

$$\frac{p_{ij}(\lambda,\lambda')}{p(\lambda)p(\lambda')}$$

where i,j specifies a neighborhood direction and λ,λ' range over the label set. For a detailed discussion of computing compatibility coefficients by mutual information see [5].

The new estimate of the probability of λ at a_i at the (k+1)st iteration is a function of both the previous estimate for that probability, $p_i^k(\lambda)$, and the contribution from the probability distributions on the neighboring label sets, $q_i^k(\lambda)$, $\forall\lambda\in\Lambda$, given by [3]

$$p_i^{(k+1)}(\lambda) = \frac{p_i^k(\lambda)[1+q_i^k(\lambda)]}{\sum_\alpha p_i^k(\alpha)[1+q_i^k(\alpha)]}$$

where

$$q_i^k(\lambda) = \sum_j \sum_\alpha r_{ij}(\lambda,\alpha)p_j(\alpha)$$

This updating scheme is useful when compatibilities are expressed as positive and negative coefficients. When compatibilities are computed by mutual information a non-negative coefficient scale results, where 0 represents high incompatibility and high values represent high compatibilities. The second model works with these compatibilities. The new estimate of the probability of λ at a_i at the (k+1)st iteration is given by [4]

$$p_i^{(k+1)}(\lambda) = \frac{p_i^k(\lambda)\sum_\alpha r_{ij}(\lambda,\alpha)p_j^k(\alpha)}{\sum_\lambda \sum_\alpha r_{ij}(\lambda,\alpha)p_i^k(\lambda)p_j^k(\alpha)}$$

When the α's at a_j are highly compatible with $p_i(\lambda)$ the sum will be high, low otherwise, and $p_i(\lambda)$ will increase relative to other p's.

Both iteration schemes yield comparable results. A study of the convergence properties of relaxation processes is found

in [6][7]. Relaxation methods have been used in breaking substitution ciphers [8], handwriting segmentation [9][19], line and curve enhancement [1][10][11] and edge enhancement [12][13], among other applications.

1.2 Blob Detection

Segmentation of objects from their background is basic to many image understanding tasks. This paper deals with the relatively simple case in which the object is a "blob". A blob can be characterized as a compact region lighter (or darker) than its background surrounded by a smoothly curved edge. Not all images conform to this rudimentary model; for example, consider images of clouds whose regions lack well defined outlines, or images that consist of subparts with differing textures. However, the model is applicable to many imaging tasks including thermal imagery analysis, chromosome classification, and industrial automation.

In principle, blobs can be extracted by thresholding the image at an appropriate level. However, if the image is noisy, thresholding will produce noisy results which may not be cleaned up in postprocessing. Thresholding may extract regions that are not bounded by edges but are smooth continuations of the background if the gray level fluctuations in the background cross the threshold level. Edge detection is also sometimes useful in object extraction. However, the edge detector may respond in the interior of the object or background as a result of noise or may fail to respond strongly on the object/background border because of blur.

Milgram [14][15] has investigated the use of edge/border coincidence as a method for object detection using the "Superslice"

algorithm. The basic concept is the matching of border points of connected components with corresponding edge values. In this approach, an edge detector is run over the image and the response thinned to an "edge map". The image is then thresholded and connected components of above-threshold points are extracted (see Rosenfeld and Kak [16] for a discussion of connected components and edge detectors). The components are accepted as objects or rejected as noise based on the coincidence of the edge map with the region boundary. This process is carried out at various thresholds and at each threshold the surviving regions are compared with the survivors of earlier thresholds. Only those regions that best match the edge map are used to describe the actual objects in the image.

Nakagawa used edge/border coincidence as an aid in edge extraction [17]. He was able to reduce the noisiness in the edge detector response by selecting those edge points that lie on region borders in the thresholded image. The selected edge points were linked into continuous curves by following the region borders.

Parikh experimented with the use of border edge strength values to determine a threshold for cloud-type objects [18]. Edge strength was defined to be the sum of the edge values for all border points of a given connected component divided by the number of border points. The border edge strength

feature failed to segment the cloud-type objects because of the ill-defined nature of the borders.

Relaxation applied to the detection of edges was successfully investigated by Schachter et al. [12]. In their approach, the gradient magnitude was computed by

$$MAG = \sqrt{(\Delta_x F)^2 + (\Delta_y F)^2}$$

where F is the image and $\Delta_x F$, $\Delta_y F$ are the x,y components of the gradient respectively. The edge direction was given by

$$\theta = \tan^{-1}\left(\frac{\Delta_y F}{\Delta_x F}\right)$$

The probability of an edge at a point (x,y) was defined by

$$p(x,y) = \frac{MAG(x,y)}{\max\limits_{u,v} MAG(u,v)}$$

where the max was taken over the entire image. $\bar{P}(x,y) = 1 - P(x,y)$ defined the no-edge probability. Edge/edge compatibility coefficients were computed based on smoothness of slope continuation for edge/edge; edge/no edge and no edge/no edge interactions were also defined. In brief, no edge reinforces no edge; edge reinforces edge if they smoothly continue one another; and edge reinforces no edge if they are alongside one another.

To apply relaxation to thresholding [21], "light" and "dark" probabilities are initially assigned to image points based on their gray levels. The probabilities are iteratively adjusted at each point based on the probabilities at the neighboring

points, i.e., light reinforces light and dark reinforces dark. This has the effect of shifting the probabilities initially assigned to noise points so as to make them more consistent with their surroundings. After a number of iterations, light probabilities should become uniformly high, and vice versa, producing a bimodal histogram with peaks at opposite ends of the gray scale, making threshold selection easier and resulting in a non-noisy binary image. However, the process still may extract regions not bounded by edges.

This thesis uses the ideas of relaxation and the ideas of edge/border coincidence in a probabilistic segmentation scheme for blob detection. Superslice, a non-probabilistic scheme, made two independent decisions based on gray level (thresholding) and edge strength (selection of maxima), then checked for coincidence to determine if an object was detected. The joint relaxation process described in this paper, on the other hand, never makes decisions. It estimates the probabilities based on gray levels and edge strengths, and then iteratively adjusts these probabilities so that both types of information are able to interact. This process thus incorporates the principle of convergent evidence in a deferred commitment scheme.

CHAPTER II

BLOB DETECTION

In this chapter we examine the edge and gray level processes operating separately, and then the joint process in which they are both combined.

2.1 Edge Relaxation

We compute the initial edge probabilities as follows. Let $e_i (i = 1,\ldots,8)$ be a measure of the gray level difference at point P in direction $45i°$, where e_i is computed by applying these masks, first proposed by Prewitt, at every picture point:

```
-1 0 1      0  1 1      1  1  1      1  1  0
-1 P 1     -1  P 1      0  P  0      1  P -1
-1 0 1     -1 -1 0     -1 -1 -1      0 -1 -1
```

We take the absolute value as the edge magnitude and let the sign indicate the edge orientation (i.e., a 90° edge is a negative 270° edge). The operator has the effect of thickening edges, i.e., producing edge responses on the leading and trailing sides of the object border. To obtain usable edge information, the output must be thinned by suppression of non-maxima of the edge magnitude in the direction across the edge at each point.

Figure 1 shows the FLIR image of a tank displayed as gray levels. Figure 2a shows the edge detector output with non-maximal responses suppressed. This illustrates the problem of

the edge detector responding to varying intensity patterns in the background. A histogram of the edge strengths is shown in Figure 2b.*

Let E be the largest e value at any point of the image, and let e_p be the largest value at point P. $p_e = e_p/E$ is taken to be an estimate of the edge probability at P and $p_n = 1-p_e$ as an estimate of the no edge probability. Further, $p_i = (e_i/s)p_e$, where $s = \sum_{i=1}^{8} e_i$, is taken as an estimate of the probability of an edge in direction 45i° at P. Thus, $\sum_{i=1}^{8} p_i = p_e$ and $p_e + p_n = 1.0$. Figure 3a shows the initial edge classifications with pixels having maximum edge probability (regardless of direction) rescaled as gray levels between 0 and 63, and pixels having maximum no edge probabilities displayed as black.

The pairwise compatibilities among $p_1,\ldots,p_8,p_n$ at adjacent points are estimated using mutual information [5]. A few of the coefficients are shown in Figure 4, showing that the relative strengths of the coefficients support the intuitive constraints of no edge reinforcing no edge, edge reinforcing edge if they smoothly continue one another, and edge reinforcing no edge (and vice versa) if they are alongside one another. This has the effect of strengthening the appropriate edge probabilities at points that lie along smooth edges, and

---

* The scale in all histogram pictures indicates the number of pixels per displayed dot.

strengthening the no edge probability elsewhere. These coefficients are used in the relaxation process of [4].

Figure 3(b-i) shows eight iterations of the edge relaxation process applied to Figure 3a. Figure 5(a-i) are the histograms of the respective iterations. As the relaxation process iterates the edge responses clustered at the lower end of the scale in Figure 2b migrate in two directions. Those points which have low edge support have increased no edge probabilities and become zero while those points receiving support have increased edge probabilities and move toward the higher values. The no edge points show up as a spike at gray level zero. The blob edge becomes significantly enhanced with the blob being completely defined after four iterations. As the process continues some of the edges in the background begin to come out; however, the improvement over Figure 2a is obvious.

2.2 Light/dark Relaxation

The light/dark process was initially designed as an automated thresholding process wherein the gray levels would decide whether they belonged to the light class or dark class. The result should be a bimodal histogram, which makes threshold selection obvious. (See [21] for a discussion of thresholding using light/dark relaxation.) In the image domain with which we are experimenting, involving homogeneous objects on a contrasting background, the light class can be equated with blob interior and the dark class with blob exterior. As it relates to edge/border coincidence, this process has the joint role of supplying the border information and classifying the object interior. The border is defined by interior points on the light sides of edges. However, we first examine the behavior of the process without the edge interaction.

We compute the initial light/dark probabilities as follows. Let g be the gray level of point P, and let b,w be the lowest and highest gray levels in the image, so that $b \leq g \leq w$ for all P. $p_w \equiv \frac{g-b}{w-b}$ is taken as the estimate of the probability that P is white, and $p_b \equiv \frac{w-g}{w-b}$ as the probability that P is black. Figure 6a shows the initial light/dark classifications of Figure 1 redisplayed as gray levels where $g = b+p_w(w-b) = w-p_b(w-b)$. Because the initial probabilities are based on gray levels and then redisplayed as gray levels, Figure 6a is a copy of the original image.

The compatibilities between the black and white classes at adjacent points are estimated using ratios of average probabilities, as in the previous section. Figure 7 shows a few of these compatibilities; we see that interior reinforces interior, exterior reinforces exterior, and adjacent interior/exterior classes are contradictory.

Figure 6(b-i) shows eight iterations of the relaxation process applied to Figure 6a. Displayed in this figure is the strength of each point's light classification. This is interpreted as the probability that each point belongs to the interior class. As the process iterates the blob interior grows. After three iterations those ambiguously classed points on the blurred edge become classified as interior. However, with no inhibitory process to temper this growth, background points neighboring the blob interior begin to accept the interior support and become classified as interior themselves. Some areas in the background which do not look blob-like (lacking smoothly curving edges) have also been somewhat enhanced. This is due to their relatively high gray level and the fact that supporting evidence is based only on gray level.

Figure 8(a-i) show the histograms of the corresponding iterations shown in Figure 6(a-i). The process produces a discrimination between the blob and the background evident by the widening valley between the exterior class, peaked at

the low end of the histogram around gray level seven, and the interior class peak gaining strength around gray level 43. A difference between the objective of this process and the thresholding process is that this produces no segmentation since no actual thresholding has been done.

2.3 Joint Relaxation

We now allow both information sources to interact in a multi-process relaxation scheme. Given the two initial sets of probabilities for each point, compatibility coefficients can be defined between p_b, p_w, $p_1,\ldots,p_8$, p_n in the same manner as in the previous sections. The edge/border interaction is embodied in the inter-process compatibilities where edge reinforces light if it is on the light side of the edge (and vice versa), edge reinforces dark if it is on the dark side of the edge (and vice versa), and the no edge/(light,dark) interations are "no information" situations. The intra-process compatibilities preserve the same reinforcement relations as previously detailed. Figure 9 is a sampling of these coefficients.

We compute adjusted probabilities using the relaxation formula by allowing the classes to interact as before but normalizing the two sets separately. At each iteration the updated light/dark estimates are normalized by

$$p_\ell = \frac{p'_\ell}{p'_b + p'_w}$$

where ℓ = b or w and p'_ℓ is the updated unnormalized estimate of ℓ, and the updated edge estimates by

$$p_k = \frac{p'_k}{p'_1 + \ldots + p'_8 + p'_n}$$

where k = (1,...,8,n).

Figure 10(a-i) shows the results of the initial classification and eight iterations of the joint relaxation process applied to Figures 3a and 6a. The figure consists of a pair of images for each iteration. In one p_w is displayed and in the other p_e is displayed. Allowing both sources of information to interact has sped up the blob edge definition. Operating in isolation, as in Figure 3, four iterations were needed to define the blob completely. Operating jointly, only three iterations are needed. The edges which come out of the background in the single process are greatly inhibited in the joint process. A comparison of Figures 2a, 3i and 10i (edge) shows a dramatic improvement. One shortcoming of the light/dark process operating alone was the blob's growth into the background. As a result of interacting with the edge information this expansion is contained, yet not entirely inhibited outside of the defined edge. The containment is most observable in the latter iterations of the process. The emergence of white patches from the background not bounded by edges is unimproved by the increased information. This is because, as can be seen from the edge process alone, there are edges in the background giving support to the light class on the light side of the edge, and no-edge probabilities have no inhibitory effect on either the light or dark probabilities.

The histograms of Figure 10(a-i) are shown in Figure 11(a-i). The effect of the joint process on the light/dark classifications

can be analytically supported by a comparison of the light/dark process histograms of this figure with the histograms of the light/dark process operating alone (Figure 8). The light/dark peaks are separated by a much sharper valley in the joint process, meaning that fewer points are ambiguously classified (relatively equal light/dark probabilities) and thus there is greater discrimination between the object and the background. The effect of the joint process on the edge/no edge classifications can also be analyzed in the light of a comparison of the edge process histograms of this figure and the histograms of the edge process operating alone (Figure 5). Although the strongest edge in the joint process is weaker than in the single process, the bulk of the edges are stronger, and the ambiguously classified edges, appearing around the low middle gray levels in the single process histogram, have been eliminated. This reflects the inhibition of edges in the background as seen in the joint gray level display.

A modification to the joint relaxation process was tried in order to deal with the problem of the blob's growth into the background. p_b and p_w are initialized based on a "borderness" measure, where p_w is initially high only adjacent to the light sides of edges and low elsewhere. (The idea that the human visual system "colors in" regions based on gray levels adjacent to their edges is well known to perception psychologists [22].)

Borderness values are computed by adding the difference value e_i (the result of applying each mask) to the points marked by 1's if $e_i > 0$, or the absolute value of e_i to the points marked by -1's if $e_i < 0$, in each of the masks shown in the previous section. The result is a set of "borderness" values which are high on the light sides of edges and low elsewhere.

p_b and p_w are initialized based on a combination of the gray level and the borderness values at each point. Let B be the maximum borderness value in the image. Let β be the borderness value at point P, and let $p_\beta = \beta/B$. Let $p_w^* \equiv \alpha p_w + (1-\alpha)p_\beta$, where $0 \leq \alpha \leq 1$ and p_w is computed as before, and let $p_b^* \equiv 1-p_w^*$.

With the edge initialization, compatibility coefficients and the relaxation process carried out as in the joint process, Figure 12(a-c) show the results of the initial classification and eight iterations with $\alpha = .5$. This is an obvious improvement over the results in Figure 10. The object definition is sharper and the emergence of light patches from the background has been effectively inhibited. Improvement has also been made in the edge classifications. The histograms of this process, Figure 13(a-i), support what is observable in the gray level display.

CHAPTER III

EXTENSIONS

This chapter discusses several extensions of the blob extraction process.

3.1 Pyramid Structure

The one-level relaxation structures of the previous chapter can be extended to a multi-level hierarchy where each successively higher level in the "pyramid" is a lower resolution image of the base image. At an appropriately resolved level blobs look like local spots, enabling immediate interaction between the blob interior and the edges on all sides. In the one-level processes a considerable number of iterations are required in order for the parts of a large blob to reinforce one another. In the pyramid structure, information passes up and down in the pyramid (inter-level interactions and intra-level interactions) facilitating faster propagation of information.

To create the gray level pyramid, on which initial class estimations are based, a base image is successively block averaged (using a 4-pixel block size), creating the lower resolution levels. Let $L_1, L_2, \ldots, L_n$ be n levels in a pyramid where L_n is a higher resolution level than L_{n+1}, and let P_{L_n} be a pixel on level n. In this structure P_{L_n} is adjacent to 13 pixels: a father in L_{n+1}, 8 brothers in L_n, and 4 sons in L_{n-1}. $P_{L_{n+1}}$ is the father of P_{L_n} (and P_{L_n} is the son of $P_{L_{n+1}}$)

if P_{L_n} was one of the 4 points averaged to compute $P_{L_{n+1}}$'s value. The 8 brothers are the 8 adjacent points of the one-level process.

Probabilities are updated by the same method as in the one level process, based on class interactions between adjacent points, but with the information from the three interacting levels weighted differently, i.e.

$$P_{L_n} = \alpha F + \beta B + \gamma S$$

where F is the father in L_{n+1}

$B \equiv \sum_{i,j} P_{(i,j)_{L_n}}$, the sum of the updated estimates of the eight brothers

$S \equiv \sum_{k,\ell} P_{(k,\ell)_{L_{n-1}}}$, the sum of the updated estimates of the four sons

and $\alpha + \beta + \gamma = 1$.

Constrained by computer memory limitations, a three-level pyramid (32x32, 16x16, 8x8) was created based on the image in Figure 1; it is shown in Figure 14. The pixels were initially classified light/dark by the process described in Chapter II and displayed in Figure 15a by the same scheme. The compatibility coefficients were computed by mutual information.

Figure 15(b-i) shows eight iterations of the light/dark pyramid process applied to Figure 15a with $\alpha = \beta = \gamma = .33$. We would expect multi-level processes to be more informed than single level processes, converging faster with more discriminative

results; however this was not the case. The multi-level process performed identically to the single-level process. Based on the rationale that the sons are less informed than their fathers, it seems reasonable that their evidence should not be allowed to reduce the class estimation. Hence weights of $\alpha = .25$, $\beta = .75$, and $\gamma = 0.$ were used, but the results were still the same.

Since this was just an initial step in the investigation of pyramidal structures for relaxation, the default option of computing compatibility coefficients by mutual information was used. A more intelligent weighting scheme might have produced better results. Other experiments are currently being conducted with multi-level processes where the higher levels determine the lower level compatibilities. Work on pyramidal structures for object extraction will be continued in the future, but is outside the scope of this thesis.

3.2 Curvature

An additional information source investigated was the use of curvature as a basis for initial estimation of "inside" and "outside" class probabilities to augment the "light" and "dark" classes in object interior/exterior interpretation. Initially, most points have equal probability of being inside or outside (assuming we do not know whether the blobs are light and the background dark or vice versa), except that points adjacent to an edge on the side away from the center of curvature have higher probability of being outside while those points on the side toward the center of curvature have higher probability of being inside. These probabilities then reinforce one another; inside reinforces inside and outside reinforces outside for neighboring pairs of points to the extent that they are not separated by an edge. Initially, the probabilities at a given point adjacent to the blob border will depend on whether the border is convex or concave at that point. Eventually, the interior of the blob should be uniformly labeled "inside" and the exterior labeled "outside" with high probability. This method can be used to label the interior of a closed curve even if it does not differ in gray level from the exterior.

A hand drawn kidney bean shaped closed curve was used to demonstrate the method; see Figure 16. The curve was chain-coded and curvature at each point was measured by computing

two slope vectors four chain links in length, one on each side of the point, normalizing each by its magnitude and taking the dot product of the vectors [20]. Using four-neighbor adjacency, those points adjacent to the edge which were toward the center of curvature were labeled "inside", and those points adjacent to the edge but away from the center of curvature were labeled "outside". The probability of belonging to each class was computed by normalizing the curvature measure at the adjacent edge by the maximum curvature value possible. If a point was adjacent to more than one edge point, supporting curvature evidence (i.e., all adjacent edge points were either convex or concave) increased class probability in proportion to the evidence strength, while contradictory curvature evidence (i.e., adjacent edge points having convex and concave measurements) created an ambiguous situation and inside/outside class probabilities were set equal. Points not adjacent to an edge were also initially assigned ambiguous, equal inside/outside probabilities. In this experiment, the edge points are known so no fuzzy classification was necessary. Edge points were assigned an edge probability of 1 and all other points assigned a 0 edge probability. Figure 17a shows the initial pixel classifications with the class probabilities rescaled as gray levels where $g = 63 - p_I*63 + .5 = p_O*63 + .5$. Initially most points are ambiguously classified and appear gray.*

*It should be pointed out that the high and low initial values at the bottom of the concavity on the right side seem to be reversed.

The compatibility coefficients for the relaxation process were determined a priori based on the constraints that inside reinforces inside and outside reinforces outside; an inside/outside label pair is contradictory, and classes separated by an edge do not interact. They are displayed in Figure 18.

Figure 17(b-m) shows twelve iterations of relaxation applied to Figure 17a. In this display scheme, as class support increases, the inside class goes to black, the outside class goes to white, and the curve remains gray. As expected, the ambiguity is resolved with the interior of the curve classified "inside" and the exterior classified "outside". The histograms of the iterations, Figure 19(a-m), show the behavior of the process. Initially, nearly all points are ambiguously classified and show up as a spike at the middle of the histogram (at value 32). As the process iterates, the spike separates with the inside class points migrating to 0 and the outside class points migrating to 63. The exterior points beyond the outwardly propagating wavefront of "outside" support and the curve points themselves remain ambiguously classified. If the process were iterated further, the entire exterior would be classified "outside" and the histogram would then consist of three spikes: an "inside" class spike at 0, an "outside" class spike at 63, and a small curve spike at 32.

Processes of this type might be used to model figure-ground ambiguity, such as the Rubin vase, by initiating a propagation

process at some particular sharply curved part of the boundary between the two regions.

3.3 Sequences of Images

Detecting objects in a time sequence of images is another domain where interacting relaxation processes may be useful. Motion between frames produces a disparity between the images. The disparity contains basic relational information about the object which aids in object definition. Information that might be difficult to extract or might even be lacking in a single image may be available in a pair of images. Joint relaxation processes can estimate the disparity or velocity at each point concurrently with the estimation of lightness/darkness and edgeness for object detection.

Presented here, for simplicity, is an example involving a one-dimensional time varying sequence where velocity is restricted to horizontal motion at unit velocity (i.e., a moving waveform). We give a model for computing class compatibilities for each pair of adjacent points at each iteration based on current class estimates involving the interactions between the light/dark process and a motion direction process. The model uses a neighborhood given by

f_{t-1}: a b c

f_t : d e f

f_{t+1}: g h i

where f_t is the frame at time t.

Let M = {N,L,R} be the set of motion direction estimations for no motion, left motion, and right motion respectively, and let G = {λ,δ} be the set of light/dark estimations. Adjacent class compatibilities are computed using the following notation. Let

$$I_2 = \begin{bmatrix} 1 & 1 \\ 1 & 1 \end{bmatrix}$$

$$I_3 = \begin{bmatrix} 1 & 1 & 1 \\ 1 & 1 & 1 \\ 1 & 1 & 1 \end{bmatrix}$$

$$S_2 = \begin{bmatrix} a & b \\ b & a \end{bmatrix}$$

$$S_3 = \begin{bmatrix} a & b & b \\ b & a & b \\ b & b & a \end{bmatrix}$$

$$J_2 = \begin{bmatrix} a' & b' \\ b' & a' \end{bmatrix}$$

$$J_3 = \begin{bmatrix} a' & b' & b' \\ b' & a' & b' \\ b' & b' & a' \end{bmatrix}$$

where a, b, a', b' are non-negative motion compatibilities with the following relative weight meanings:

a	compatible
b	incompatible
a'	highly compatible
b'	highly incompatible

and I_2, I_3 are "no information" compatibility matrices.

Let $A \equiv NS_2 + (L+R)I_2$

$B \equiv |\lambda-\lambda'|I_3 + (1-|\lambda-\lambda'|)S_3$

$C \equiv NJ_2 + (L+R)I_2$

$D \equiv RJ_2 + NS_2 + LI_2$

$E \equiv NJ_3 + (L+R)B$

$G \equiv RJ_3 + LI_3 + NB$

The formulas are used as shown in the following tables to compute the compatibility coefficients for the designated neighboring points.

e \ d	λ	δ	L	R	N
λ	A		I		
δ					
L	I		B		
R					
N					

Table 1

e \ b	λ	δ	L	R	N
λ	C		I		
δ					
L	I		E		
R					
N					

Table 2

e^a	λ	δ	L	R	N
λ	D		I		
δ					
L	I		G		
R					
N					

Table 3

where I denotes the "no information" coefficients.

The principle behind these computations is to base the light/dark compatibility coefficients on the motion estimations of the point, and base the motion compatibility coefficients on the gray level similarity of the adjacent points. The coefficients calculated by these tables conform to the constraints that points moving with similar motion reinforce each other if they are both within the object or background, interior reinforces interior, exterior reinforces exterior, and motion from the object should not propagate to the background. Table 1 shows the intraframe computation. Table 2 shows the "no motion" situation where point b in frame f_{t-1} becomes point e in f_t. Table 3 shows the "right motion" case where point a in frame f_{t-1} becomes point e in f_t. The computations of coefficients for the other adjacent points are based on these three tables with the obvious symmetrical relations and appropriate direction substitutions.

CHAPTER IV

CONCLUSION

We have examined a fuzzy classification scheme for blob detection which bases its classification updating on edge and gray level information. We examined the processes operating both independently and together. We also discussed extensions to these processes and to the problem domain.

The edge relaxation process operating independently defined the object after four iterations, but with some edges being brought out of the background as the process continued. However, the results were an improvement over the non-probabilistic edge detector results. Interacting with the light/dark information resulted in further inhibition of the background edges that did not surround a blob, and yielded complete blob definition in fewer iterations. The borderness scheme further improved the results producing an almost perfect segmentation.

In the light/dark relaxation process operating independently the blob interior grew into the background. Interaction with the edge information substantially contained the interior growth and produced an improved object/background discrimination. In the borderness scheme the object interior grew inwards filling the object and resulting in a further object/background discrimination.

Under the premise that multi-level processes have faster information propagation and are more informed than single level processes we tried relaxation on a pyramid structure of successively resolved images. As this was the first stage of experimentation, we tried the default option of computing compatibility coefficients by mutual information. The results were no improvement over the single level process. The next step appears to be choosing more intelligent coefficients to support the object information.

Using curvature to provide an initial estimate of inside/outside probabilities produced an accurate classification on our experimental curve. Now that we have verified its behavior, this information source should be brought to interact with the edge and gray level processes. The additional information should produce a still sharper object/background discrimination.

We also formulated a parallel model for computing compatibility coefficients for blob detection in a time sequence of images. We restricted motion to its simplest case, horizontal unit motion in one dimension, to study the object position/movement relations in successive frames. The model is untested as yet because of the computational cost involved. As the position/movement relations become better understood, they can be generalized to less restricted domains.

All of the processes examined in this paper are parallel processes. At present, the time requirements for these processes limit their usefulness as real-time object detectors. However, with the development of parallel processors the computational cost involved should well be within the requirements of real-time object detection.

REFERENCES

1. Zucker, "Relaxation Labeling and the Reduction of Local Ambiguities", Proc. Third International Joint Conference on Pattern Recognition, San Diego, Calif., Nov. 1976, pp. 852-861.

2. Rosenfeld, "Iterative Methods in Image Analysis", Proc. IEEE Conference on Pattern Recognition and Image Processing, N.Y., June 1977, pp. 14-18.

3. Rosenfeld, Hummel, Zucker, "Scene Labeling by Relaxation Operations", IEEE Trans. on Systems, Man, and Cybernetics, SMC-6, 1976, pp. 420-433.

4. Peleg, "A New Probabilistic Relaxation Scheme", TR-711, Comp. Sci. Center, Univ. of Md., Nov. 1978.

5. Peleg, Rosenfeld, "Determining Compatibility Coefficients for Curve Enhancement Relaxation Processes", IEEE Trans. on Systems, Man, and Cybernetics, SMC-8, 1978, pp. 548-555.

6. Zucker, Krishnamurthy, Haar, "Relaxation processes for Scene Labeling: Convergence, Speed, and Stability", IEEE Trans. on Systems, Man, and Cybernetics, SMC-8, 1978, pp. 41-48.

7. Eklundh, Rosenfeld, "Convergence Properties of Relaxation", Comp. Sci. Center, Univ. of Md., TR-701, Oct. 1978.

8. Peleg, Rosenfeld, "Breaking Substitution Ciphers Using a Relaxation Algorithm", Comp. Sci. Center, Univ. of Md., TR-721, Jan. 1979.

9. Peleg, "Ambiguity Reduction in Handwriting with Ambiguous Segmentation and Uncertain Interpretation", Comp. Sci. Center, Univ. of Md., TR-724, Jan. 1979.

10. Davis, Rosenfeld, "Curve Segmentation by Relaxation Labeling", IEEE Trans. on Computers, C-26, 1977, pp. 1053-1057.

11. Danker, Rosenfeld, "Strip detection Using Relaxation", Pattern Recognition, to be published.

12. Schachter, Lev, Zucker, and Rosenfeld, "An Application of Relaxation Methods to Edge Reinforcement", IEEE Trans. on Systems, Man, and Cybernetics, SMC-7, 1977, pp. 813-816.

13. Peleg, Rosenfeld, "Straight Edge Enhancement and Mapping", Comp. Sci. Center, Univ. of Md., TR-694, Sept. 1978.

14. Milgram, "Region Extraction Using Convergent Evidence", Proceedings Image Understanding Workshop, April 1977, pp. 58-64.

15. Milgram, "Progress Report on Segmentation using Convergent Evidence", Proceedings Image Understanding Workshop, Oct. 1977, pp. 104-108.

16. Rosenfeld, Kak, Digital Picture Processing, Academic Press, N.Y., 1978.

17. Nakagawa, Rosenfeld, "Edge/Border Coincidence as an Aid in Edge Extraction", IEEE Trans. on Systems, Man, and Cybernetics, SMC-8, 1978, pp. 899-901.

18. Parikh, Rosenfeld, "Automatic Segmentation and Classification of Infrared Meteorological Satellite Data", IEEE Trans. on Systems, Man, and Cybernetics, SMC-8, 1978, pp. 736-743.

19. Hayes, "Reading Handwritten Words Using Hierarchical Relaxation", Ph.D. Dissertation, Computer Science Dept., University of Maryland, College Park, Md., 1979.

20. Rutkowski, Rosenfeld, "A Comparison of Corner-Detection Techniques for Chain-Coded Curves", Comp. Sci. Center, Univ. of Md., TR-623, Jan. 1978.

21. Smith, "General Purpose Software Package for Array Relaxation", M.S. Thesis, Computer Science Dept., University of Md., College Park, Md., 1979.

22. Cornsweet, Visual Perception, Academic Press, N.Y., 1970.

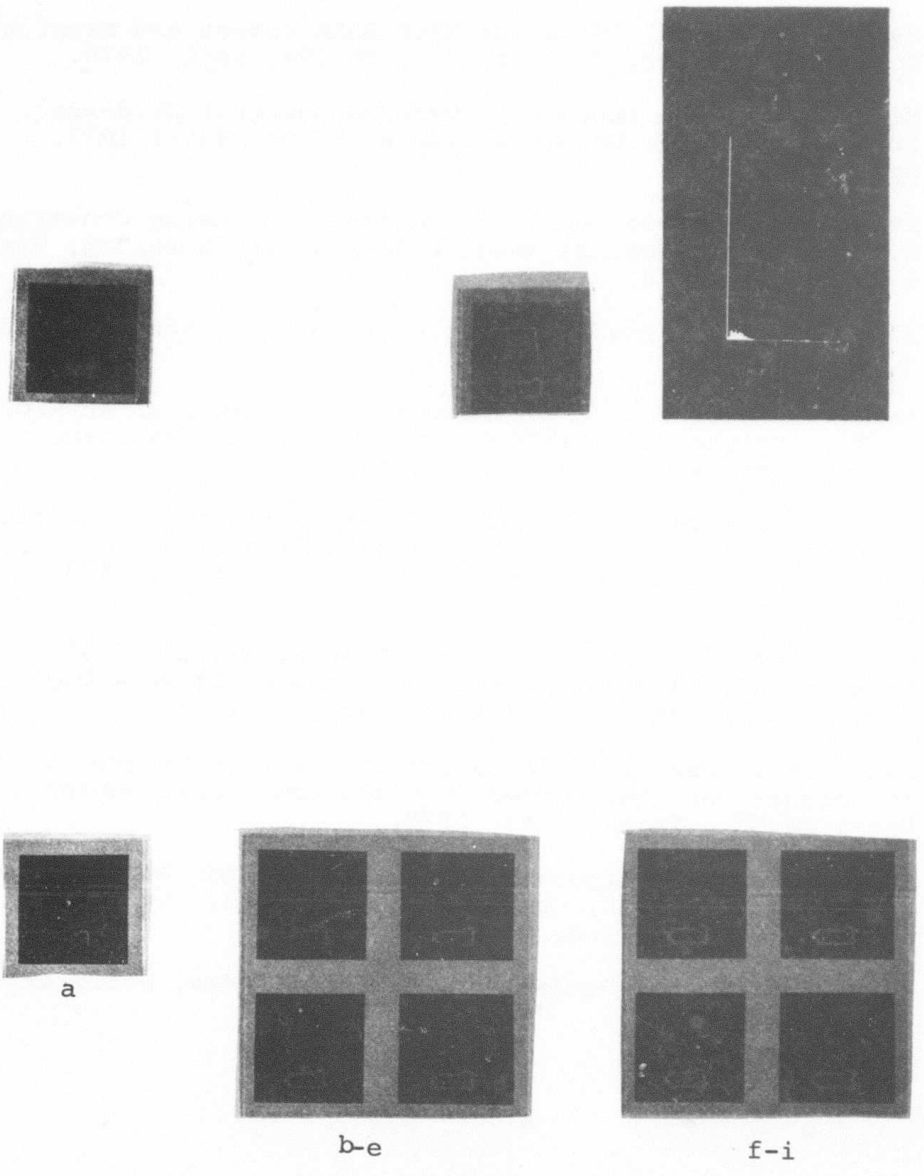

Fig. 3 a) Initial edge/no edge classifications of Fig. 1.
b-i) Eight iterations of relaxation applied to Fig. 3a.

label[p] : →	label[nbr] : →		label[p] : →	label[nbr] : ↖	
3.449571	2.735268	2.989768	0.618779	1.834991	0.656950
13.303496	p	13.303496	0.094431	p	0.600613
2.989768	2.735268	3.449571	0.137451	0.153977	0.163758

label[p] : →	label[nbr] : ←		label[p] : →	label[nbr] : ↗	
0.069581	0.219511	0.164322	1.907638	4.107503	4.381657
0.002263	p	0.003521	8.935122	p	10.084600
0.030989	0.045222	0.031845	2.596691	2.433852	2.016059

label[p] : →	label[nbr] : ↑		label[p] : →	label[nbr] : ↙	
1.036540	4.441962	3.797525	1.078657	0.947074	0.652277
1.751447	p	3.200273	0.200243	p	0.129268
0.914150	1.432359	0.398709	0.025246	0.162744	0.088019

label[p] : →	label[nbr] : ↓		label[p] : →	label[nbr] : NE	
4.106131	2.371873	1.064473	0.868406	0.891125	0.875631
4.828966	p	3.729727	0.686561	p	0.674626
0.525983	1.328874	1.809332	0.919590	0.954691	0.906917

label[p] : →	label[nbr] : ↘	
4.723255	2.132231	0.993537
12.241382	p	11.387216
2.307259	2.240219	3.518801

Fig. 4. Examples of compatibility coefficients for edge relaxation. The edge → is a light/dark → edge with the other edges rotations of it.

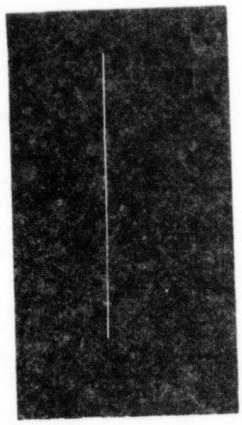

a

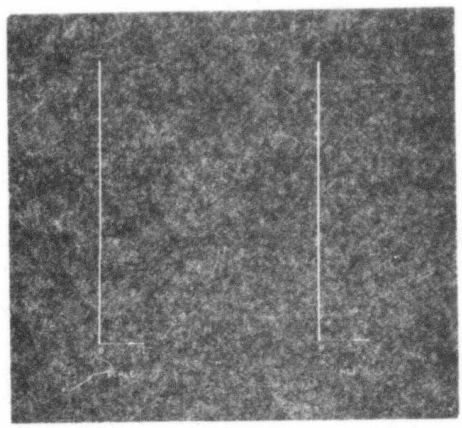

b c

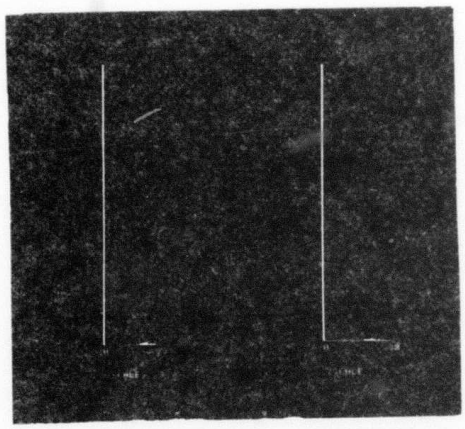

d e

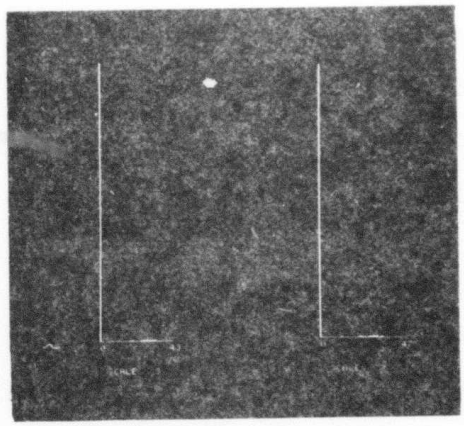

f g

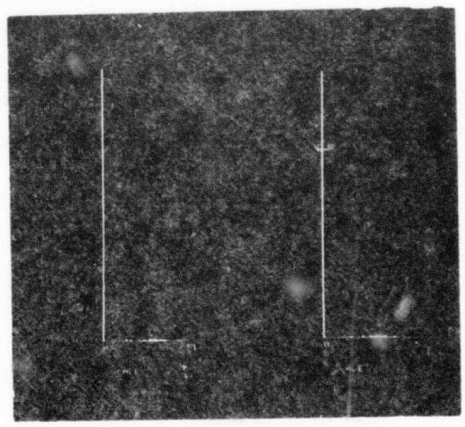

h i

Fig. 5 a-i) Histograms of Fig. 3 (a-i)

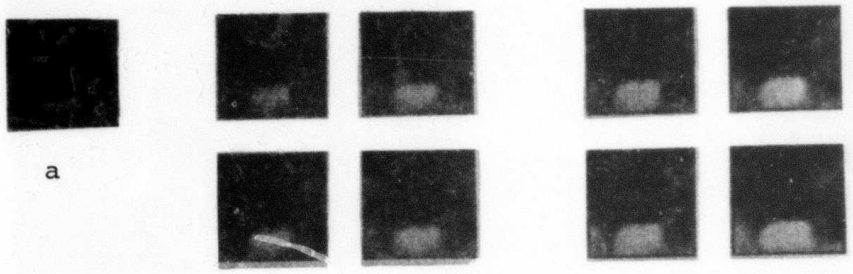

Fig. 6 a) Initial light/dark classifications of Fig. 1.
b-i) Eight iterations of relaxation applied to Fig. 6a.

label[p] : Light		label[nbr] : Light	label[p] : Dark		label[nbr] : Light
1.899474	1.911622	1.861720	0.878841	0.863841	0.872712
1.908425	p	1.889212	0.833591	p	0.825634
1.802868	1.831607	1.800759	0.809413	0.792967	0.799459

label[p] : Light		label[nbr] : Dark	label[p] : Dark		label[nbr] : Dark
0.823850	0.821471	0.831243	1.023727	1.026665	1.024928
0.822097	p	0.825860	1.032589	p	1.034147
0.842769	0.837141	0.843182	1.037324	1.040545	1.039273

Fig. 7. Compatibility coefficients for light/dark relaxation.

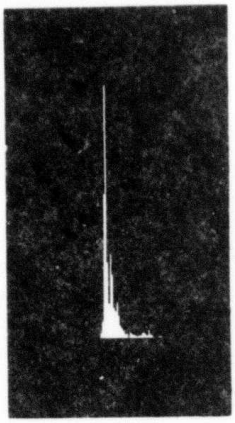

a

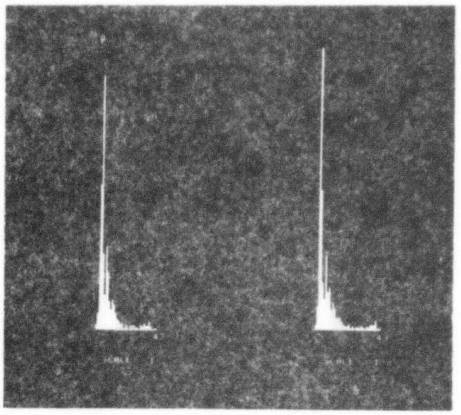

b c

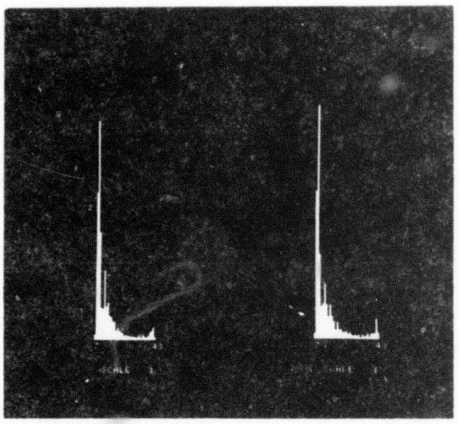

d e

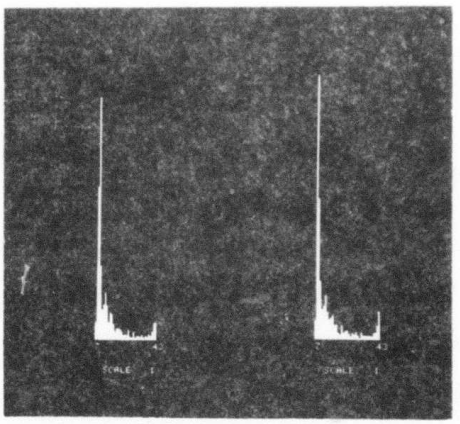

f g

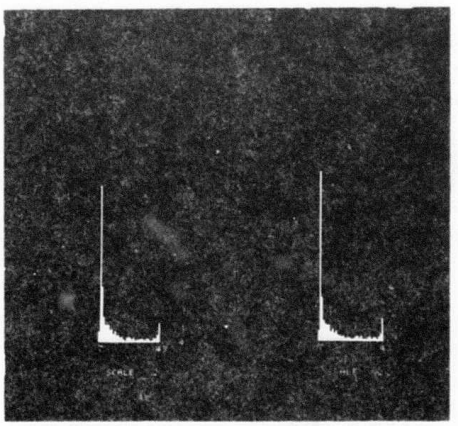

h i

Fig. 8 a-i) Histograms of Fig. 6 (a-i)

label[p] : Light	label[nbr] : →		label[p] : Dark	label[nbr] : →	
0.935456	0.979661	0.941326	0.988469	0.994717	0.960597
0.814138	p	0.825806	1.709483	p	1.659618
0.638911	0.652284	0.641232	2.455052	2.620640	2.460205

label[p] : Light	label[nbr] : ↑		label[p] : Dark	label[nbr] : ↑	
0.932524	0.803443	0.607502	1.199085	1.884802	2.240233
0.947256	p	0.585945	1.237704	p	2.469181
0.900551	0.770539	0.580406	1.217793	1.898205	2.286948

label[p] : Light	label[nbr] : ↘		label[p] : Dark	label[nbr] : ↘	
0.886375	0.987558	1.002437	1.119594	0.979270	0.820992
0.758947	p	0.920270	1.849878	p	1.320164
0.602609	0.700845	0.756032	2.487267	2.366656	1.997890

label[p] : Light	label[nbr] : ↙		label[p] : Dark	label[nbr] : ↙	
0.610647	0.699178	0.757497	2.559976	2.421634	2.103482
0.719115	p	0.872555	2.120563	p	1.616848
0.748469	0.841446	0.855027	1.534926	1.373878	1.270607

label[p] : Light	label[nbr] : NE		label[p] : Dark	label[nbr] : NE	
0.943953	0.978146	0.945335	0.880897	0.902736	0.877210
0.974432	p	0.975667	0.927173	p	0.924237
0.941775	0.975762	0.942862	0.901072	0.923959	0.897943

Fig. 9. Examples of compatibility coefficients for joint relaxation.

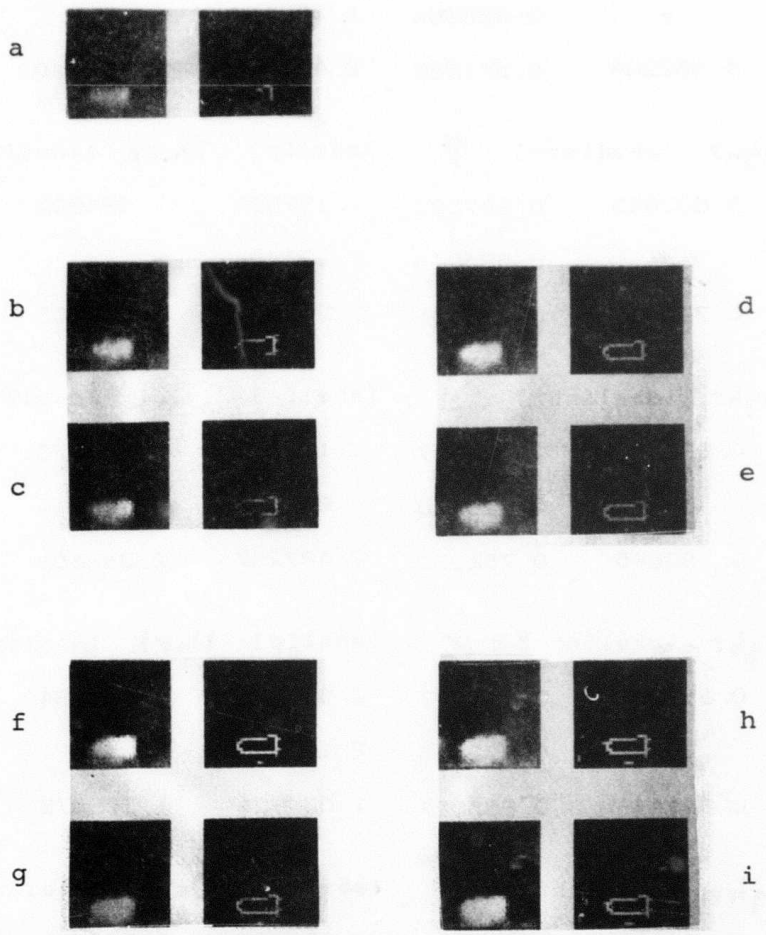

Fig. 10 a) Initial (edge/no edge)/(light/dark) classification of Fig. 1.
b-i) Eight iterations of relaxation applied to Fig. 10a.

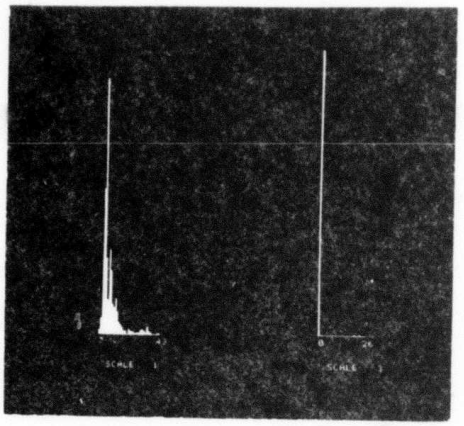

a

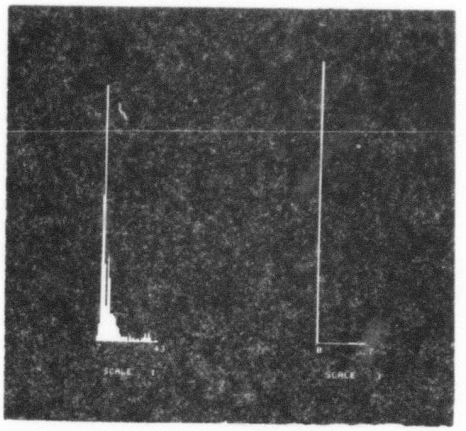

b

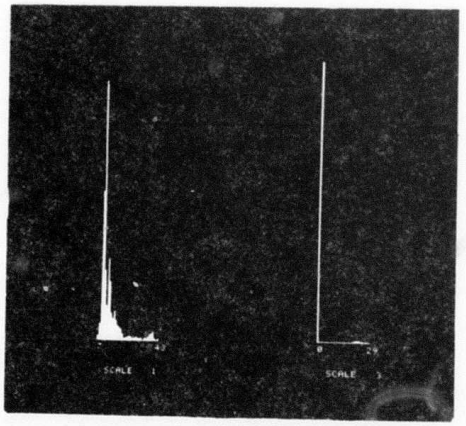

c

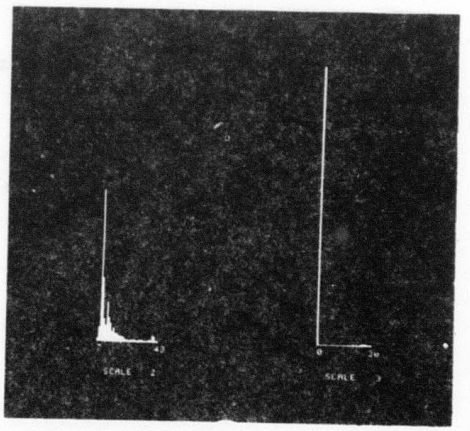

d

Fig. 11 (a-i) Histograms of Fig. 10 (a-i).

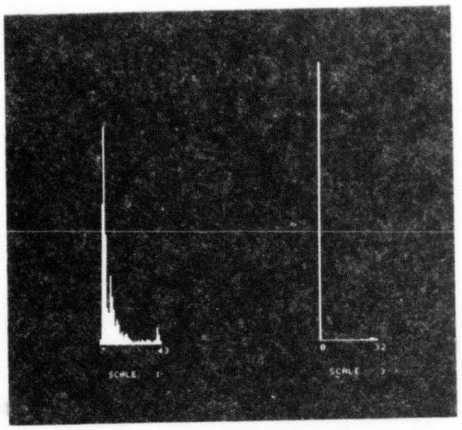

e

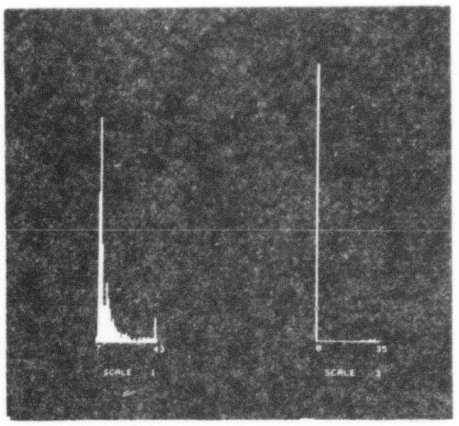

f

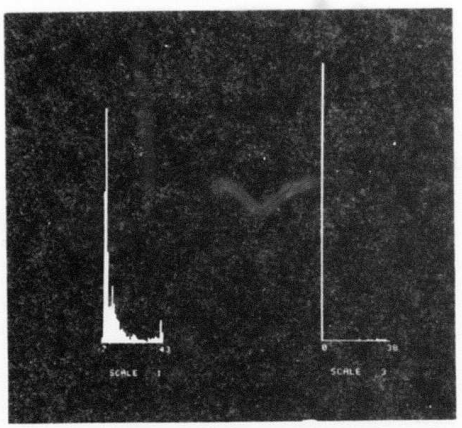

g

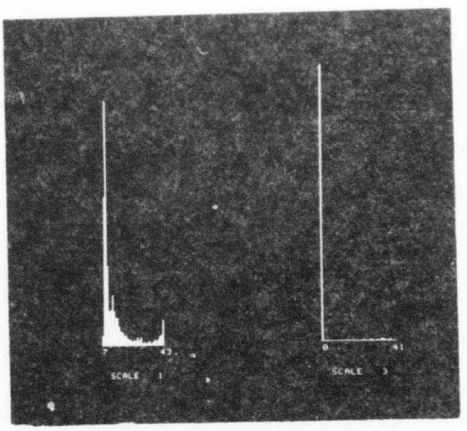

h

Fig. 11 continued

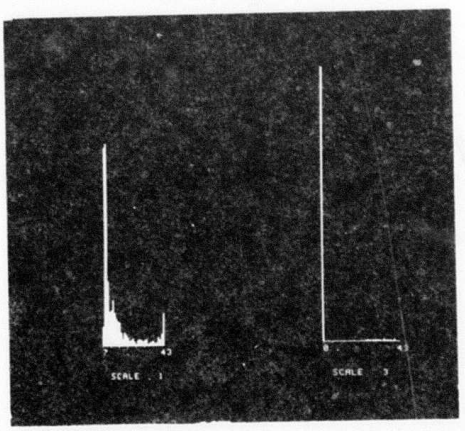

i

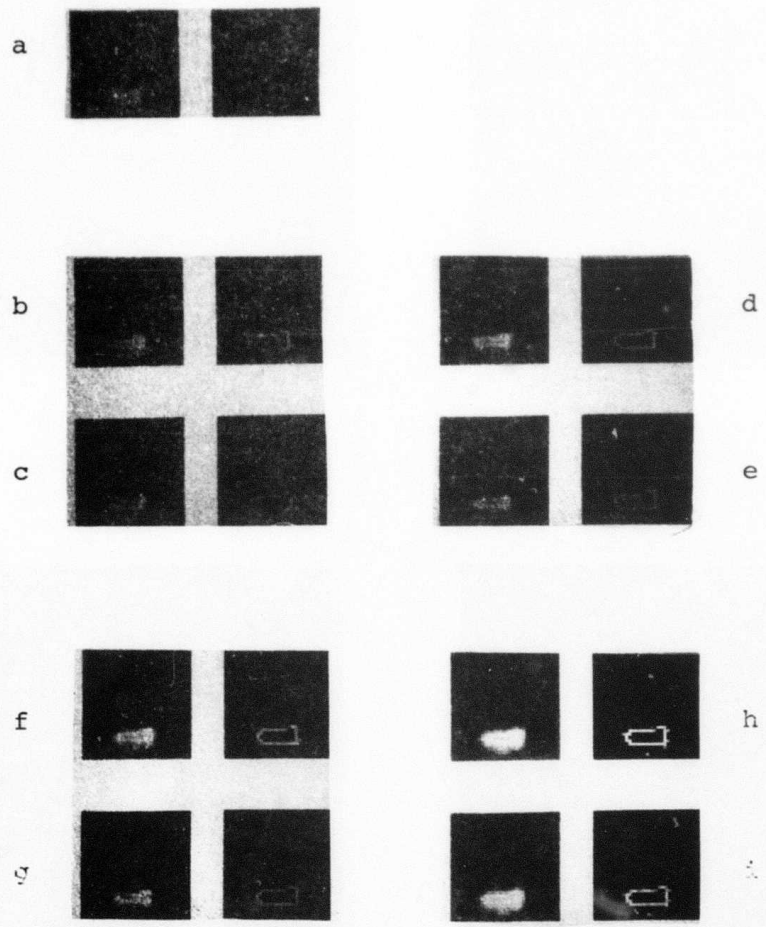

Fig. 12 a) Initial borderness classifications of Fig. 1.
b-i) Eight iterations of relaxation
applied to Fig. 12a.

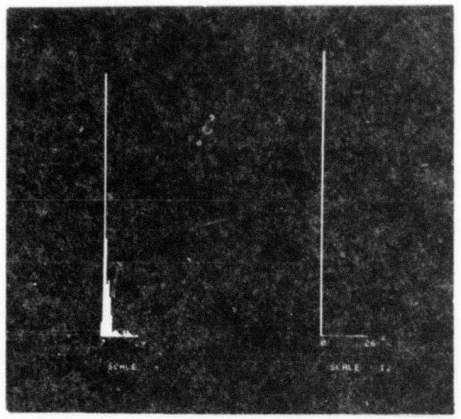

a

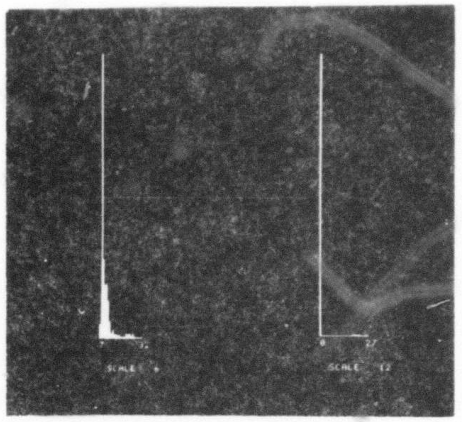

b

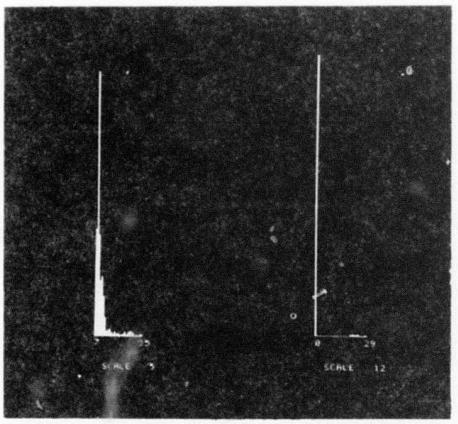

c

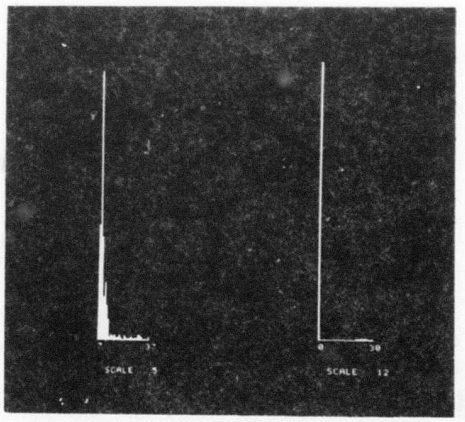

d

Fig. 13 (a-i) Histograms of Fig. 12 (a-i).

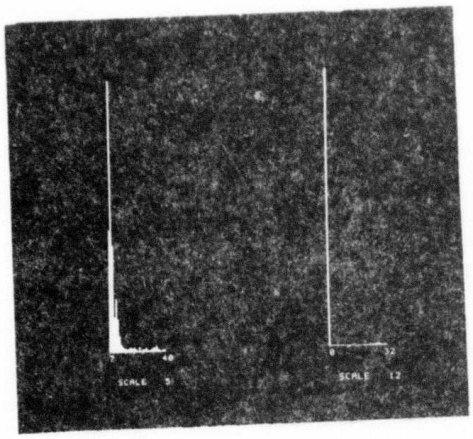

e

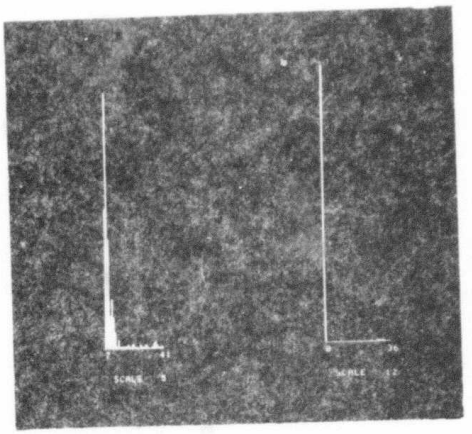

f

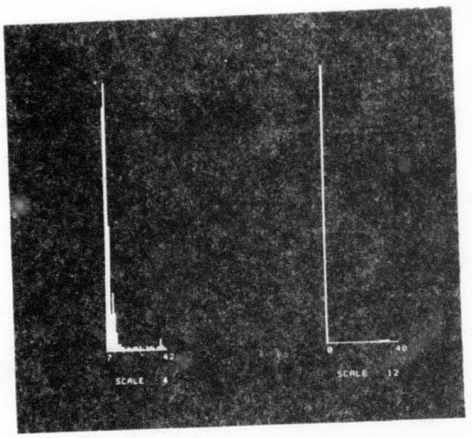

g

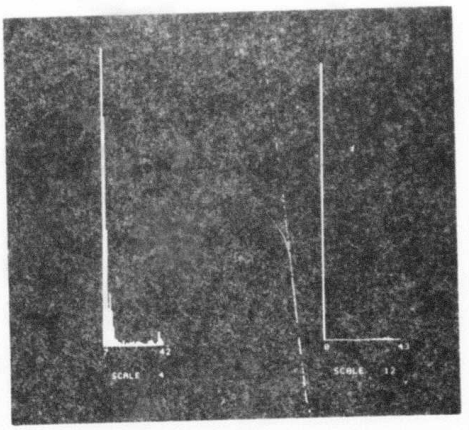

h

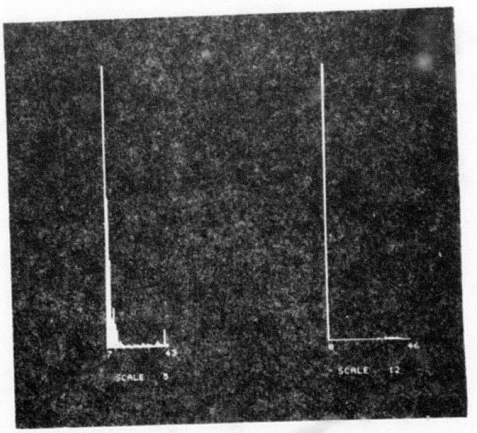

i

Fig. 13 continued

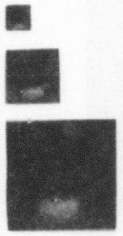

Fig. 14. Gray level pyramid.

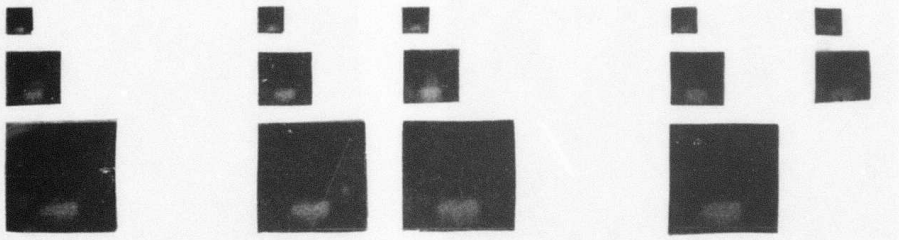

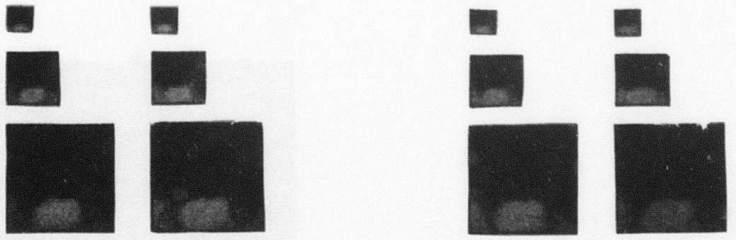

Fig. 15 a) Initial light/dark pyramid classifications of Fig. 14.
b-i) Eight iterations of relaxation applied to Fig. 15a.

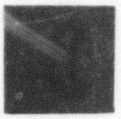

Fig. 16. Curve.

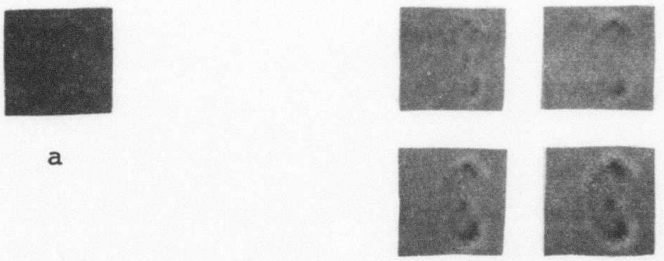

a

b-e

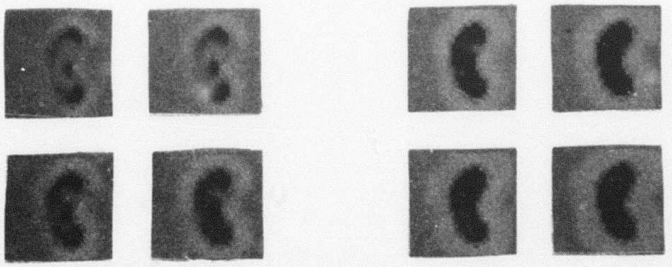

f-i

j-m

Fig. 17 a) Initial inside/outside classifications of Fig. 16.
b-m) Twelve iterations of relaxation applied to Fig. 17a.

Inside	Inside	6.0
Inside	Outside	0.
Inside	Edge	.5
Outside	Inside	0.
Outside	Outside	6.0
Outside	Edge	.5
Edge	Inside	.5
Edge	Outside	.5
Edge	Edge	.5

Fig. 18. Compatibility coefficients for inside/outside relaxation.

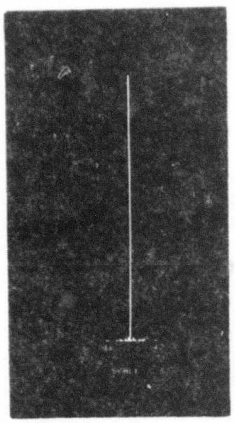

a

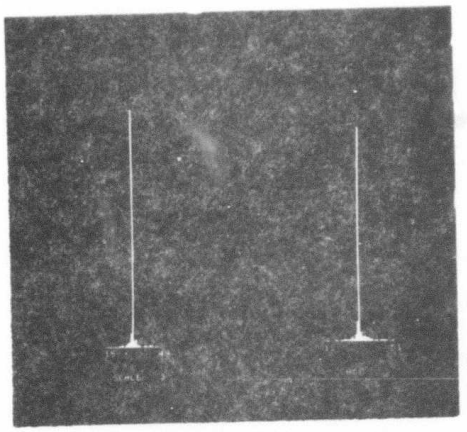

b c

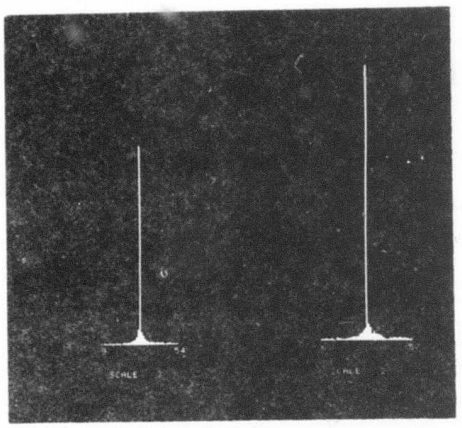

d e

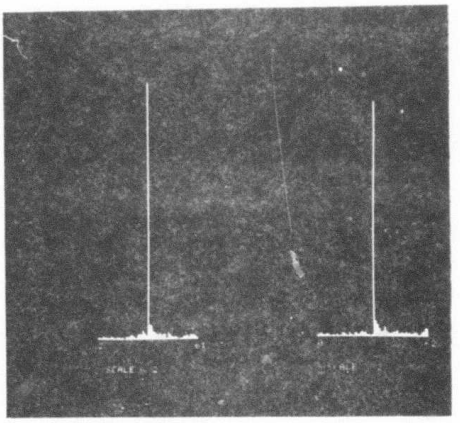

f g

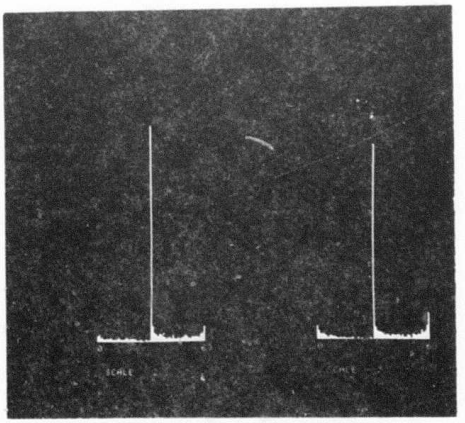

h i

Fig. 19 a-i) Histograms of Fig. 17 (a-m)

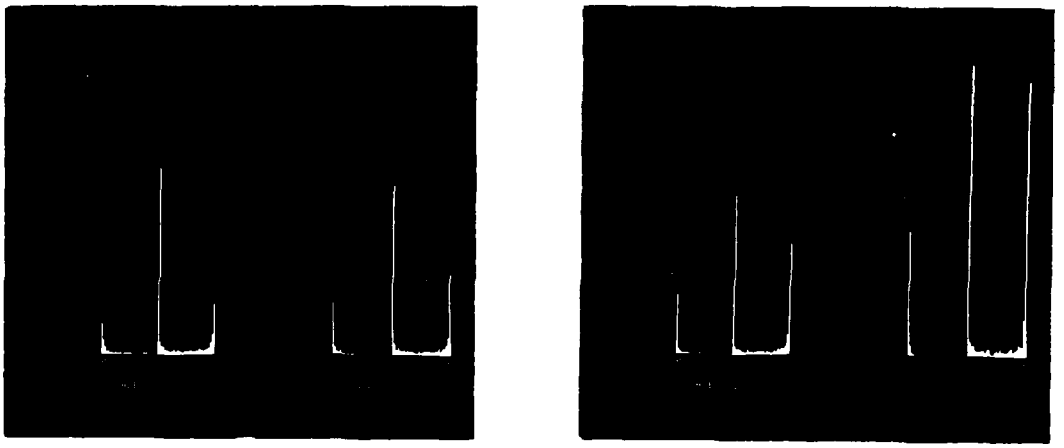

j k l m

Fig. 19 continued.

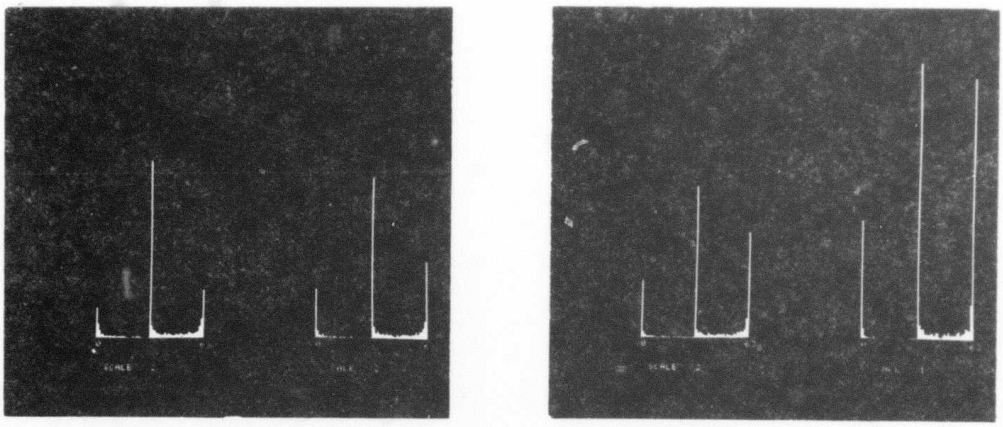

j k l m

Fig. 19 continued.

UNCLASSIFIED

SECURITY CLASSIFICATION OF THIS PAGE (When Data Entered)

REPORT DOCUMENTATION PAGE

READ INSTRUCTIONS BEFORE COMPLETING FORM

1. REPORT NUMBER

2. GOVT ACCESSION NO. AD-A086790

3. RECIPIENT'S CATALOG NUMBER

4. TITLE (and Subtitle)
(6) BLOB DETECTION BY RELAXATION,

5. TYPE OF REPORT & PERIOD COVERED
(9) Technical Rept.

6. PERFORMING ORG. REPORT NUMBER
(14) TR-795

7. AUTHOR(s)
(10) Alan/Danker
Azriel/Rosenfeld

8. CONTRACT OR GRANT NUMBER(s)
DAAG-53-76C-0138

9. PERFORMING ORGANIZATION NAME AND ADDRESS
Computer Science Center
University of Maryland
College Park, MD 20742
(11) Jul 79

10. PROGRAM ELEMENT, PROJECT, TASK AREA & WORK UNIT NUMBERS
(12) 57

11. CONTROLLING OFFICE NAME AND ADDRESS
U.S. Army Night Vision Laboratory
Fort Belvoir, VA 22060

12. REPORT DATE
July 1979

13. NUMBER OF PAGES
54

14. MONITORING AGENCY NAME & ADDRESS(if different from Controlling Office)

15. SECURITY CLASS. (of this report)
Unclassified

15a. DECLASSIFICATION/DOWNGRADING SCHEDULE

16. DISTRIBUTION STATEMENT (of this Report)

Approved for public release; distribution unlimited.

17. DISTRIBUTION STATEMENT (of the abstract entered in Block 20, if different from Report)

(15) DAAG53-76-C-0138, DARPA Order-3206

18. SUPPLEMENTARY NOTES

19. KEY WORDS (Continue on reverse side if necessary and identify by block number)

Image processing
Pattern recognition
Segmentation
Thresholding
Edge detection
Relaxation

20. ABSTRACT (Continue on reverse side if necessary and identify by block number)

A blob is a compact region lighter (or darker) than its background surrounded by a smoothly curved edge. Blobs can be detected using cooperating relaxation processes to enhance their interior and edge probabilities. A discussion of the processes working independently and together is given. The use of a pyramidal relaxation structure, the use of the closedness of contours as an additional information source, and the → next page

DD FORM 1 JAN 73 1473 EDITION OF 1 NOV 65 IS OBSOLETE

UNCLASSIFIED 411074

SECURITY CLASSIFICATION OF THIS PAGE (When Data Entered)

Abstract (continued)

extension of cooperating relaxation processes to a time sequence of images are also discussed.